RSC Advances

PAPER

View Article Online
View Journal | View Issue

Cite this: *RSC Adv.*, 2020, **10**, 10816

Intrinsic defect engineered Janus MoSSe sheet as a promising photocatalyst for water splitting

Yimin Xu,[a] Yongsheng Yao,[a] Wenjin Yin,[bc] Juexian Cao,[a] Mingyang Chen[cd] and Xiaolin Wei *[a]

Received 6th January 2020
Accepted 5th March 2020

DOI: 10.1039/d0ra00119h

rsc.li/rsc-advances

The Janus MoSSe sheet has aroused significant attention due to its band edge position and intrinsic dipole moment, making it a strong candidate for water splitting photocatalysis. However, weak water adsorption seriously prevents its further application. Here, first-principles calculations are used to explore the effect of intrinsic defects on water adsorption and conversion at the Janus MoSSe sheet. First-principles calculation results clearly show that intrinsic defects (S_{vac}, Mo_{anti}, and Mo_{int}) can effectively alter the interaction between water and the MoSSe sheet. Except for S_{vac} defects, the adsorption energy of water at Mo_{anti} or Mo_{int} defects can be significantly increased by −1.0 to −1.5 eV with respect to the weak water adsorption on a pristine MoSSe sheet of about −0.24 eV. More importantly, the energy barrier for water conversion can be dramatically lowered by 48% to 0.7 eV at Mo_{anti} or Mo_{int} defects, together with a more stable final state. Such significant enhancement of the adsorption energy is attributed to the red shift of water energy levels, resulting from the strong interaction between O2p orbitals and Mo3d orbitals. It is shown that the intrinsic defects have the potential to change the photocatalytic reactivity of the surface, and thus this may serve as an important way to design photocatalysts for water splitting.

Introduction

Photocatalytic water splitting is gaining increased interest, since it is a promising "green chemistry" approach for the direct conversion of water into clean energy H_2 driven by solar light.[1–3] However, low-efficiency production of H_2 seriously prevents its further applications. Thus, it is urgent to search for a photocatalyst with high stability and efficiency. As a potential photocatalyst, several key criteria should be satisfied as follows. Firstly, a suitable band gap larger than 1.23 eV is required for the photocatalyst to harvest the solar light.[4] Then, the photocatalyst must have decent band edge positions for overall water splitting, with the conduction band minimum (CBM) higher than the reduction potential ($E_{H^+}/E_{H_2} = -4.44$ eV) and valence band maximum (VBM) lower than the oxidation potential ($E_{O_2}/E_{H_2O} = -5.67$ eV). In addition, separation of the photogenerated electron–hole pair is also a crucial factor to reduce the possibility of carrier recombination.[5]

Based on the above criteria, various semiconductors including TiO_2, ZnO, CdS, Fe_2O_3, Bi_2WO_6, Cu_2O, *etc.* have been proposed as photocatalysts to increase the efficiency for water splitting.[1,6] However, some of these photocatalysts such as TiO_2 are inactive for overall water splitting into O_2 and H_2 in the absence of sacrificial reagents because of a large band gap and low quantum efficiency.[7] Recently, low dimensional materials have also aroused extensive attention due to the fundamental properties such as large surface area, tunable electronic structure, and abundant reactive sites.[8–12] For example, researchers have found that two dimensional g-C_3N_4, and transition metal dichalcogenides (TMDs) have suitable band gaps and robust absorption in the solar spectrum, which is suitable for water splitting.[13–15] Especially, it has reported that TMDs such as MoS_2 exhibits a direct band gap of about 1.9 eV as it is tailored into single layer, and the band edge can across the reduction and oxidation potential of water splitting.[16,17] However, the carrier mobility of electron and hole in the pristine MoS_2 is relatively low, leading to the low efficiency in water splitting activity and hindering its further applications.[18–20]

Except for the traditional TMDs, forming a Janus structure is also an efficient strategy to enhance the physical and chemical properties of the materials.[21,22] For example, Guo *et al.* found that the Janus group III chalcogenide structure could greatly enhance the piezoelectric effect associated with the intrinsic dipole perpendicular to the plane structure.[23] Furthermore, the enhanced dipole of the Janus structure can generate an intrinsic electric field, which facilitates the separation of the photogenerated carriers in the photocatalytic reactions.[24] On the other hand, some researches have proposed some new Janus

[a]*Department of Physics and Laboratory for Quantum Engineering and Micro-Nano Energy Technology, Xiangtan University, Xiangtan 411105, Hunan, China. E-mail: xlw@xtu.edu.cn*

[b]*School of Physics and Electronic Science, Hunan University of Science and Technology, Xiangtan 411201, China*

[c]*Beijing Computational Science Research Center, Beijing 100084, China*

[d]*School of Materials Science and Engineering, University of Science and Technology Beijing, Beijing 100083, China*

structures with excellent photocatalytic property. For example, Yang *et al.* have proposed a novel family of Janus single-layer group-III monochalcogenides (J–MX, J = Ga, M = In, X = S and Se) using first-principles calculations, and found their band gaps are suitable for water photocatalytic splitting.[25] And Gao *et al.* also proposed eight IV–V compound materials showing excellent photocatalysts for water splitting reactions with high efficiency of visible light.[26]

Recently, Lu *et al.* have grown a Janus monolayer of transition metal dichalcogenides named MoSSe through breaking the out-of-plane structural symmetry of the single layer MoS_2.[27] Janus MoSSe is structurally viewed as MoS_2 with all of S atoms on one side replaced by Se atoms, and exhibits an electronic structure similar to that of MoS_2.[28] Unlike MoS_2, an intrinsic dipole exists along the vertical direction of the MoSSe structure, and Yin *et al.* have found the carrier mobility of Janus MoSSe structure could be greatly affected by the dipole and layer thickness by DFT calculation.[29] Further HSE06 result proposed by Ma *et al.* shows that the Janus MoSSe sheet can be a potential water splitting photocatalyst with wide solar-absorption range and retard carrier recombination.[30] Based on the above results, other works on photocatalytic water splitting have been performed. For example, using HSE06+SOC method, Din *et al.* found that the appropriate band alignments for visible light water splitting can be achieved through forming MoSSe/GeC heterostructure.[31] Further study showed that despite the band gaps of MoSSe/XN (X = Al, Ga) heterostructures being smaller than 1.23 eV, the band edge positions are always suitable for visible-infrared water splitting.[32] On the other hand, Guan *et al.* found that few layer Janus MoSSe are suitable for visible light water splitting through thickness administrating.[33] Therefore, it can be deduced that Janus MoSSe related materials can be excellent photocatalysis for water splitting. Unfortunately, the adsorption energy of molecular water at pristine MoSSe sheet is about 0.16 eV, suggesting an extremely weak van der Waal (vdW) interaction similar to CO_2 adsorption at TiO_2 surface,[34,35] which will seriously hinder the process of water conversion.

So far, to enhance the adsorption of molecular species at the surface, there are several approaches such as surface modification, transition metal or nonmetal doping, and defect introduction.[36–39] Among these methods, introducing intrinsic defect may be superior to other approaches.[40] First, intrinsic defects are inevitable during the material growth and are also difficult to eliminate. Furthermore, defect introduction can not only vary the reactivity of the local surface structure, but also change the electronic structure of the material. For example, Zhang *et al.* reported that the band gap and work function of monolayer Janus MoSSe can be modified by simple hydrogenation method.[41] On the other hand, during the photon related process, the presence of defects can change the quantum yield of photonic excitation by tuning the energy band structure, modifying electron–hole separation, and carrier transport property.[42] For example, it has been reported that chalcogenide vacancy exists at TMDs.[43] Chaurasiya *et al.* have found that intrinsic defects can effectively alter the adsorption behaviors of NO_2, NO, and NH_3 on Janus MoSSe sheet.[44] However, the detailed role of the intrinsic defects on introducing the adsorption state and enhancing the photoreaction of water is still unknown.

The purpose of this work is to unveil the effects of intrinsic defects on water splitting at Janus MoSSe sheet. Particular attention will be focused on the following questions: (i) What is the most stable configuration of the Janus MoSSe sheet with intrinsic defects like? (ii) What effects do the intrinsic defects have on water adsorption and conversion? (iii) What factors are crucial to govern the interaction between water and substrate? Our results clearly show that Mo_{anti} defect favors forming two Mo–S bonds and two Mo–Mo bonds, while Mo_{int} favors be located over lattice Mo site. The adsorption and conversion of water can be strongly enhanced by intrinsic defects. Thus, intrinsic defect introduction exhibits great potential for the design of photocatalysis for water splitting.

Computational method

The first-principles calculations were conducted by the spin-polarized density functional theory (DFT) within periodic boundary conditions, as implemented in the CP2K/Quickstep package.[45] The CP2K implementation of DFT employs the hybrid Gaussian and plane wave (GPW) basis sets and the norm conserving Goedecker–Teter–Hutter pseudopotentials to describe the ion–electron interactions.[46] The Gaussian functions consisting of a double-ζ plus polarization (DZVP) basis set was used for all calculations. Perdew–Burke–Ernzerhof (PBE) functional was employed for the exchange-correlation term based on the generalized gradient approximation (GGA).[47] The energy cutoff for the real space grid was set at 500 Ry, which yields total energies converged to at least 0.001 eV per atom. Reciprocal space sampling was restricted to the Γ-point, due to the rather large size of the used simulation cells. To consider the weak interaction between water and Janus MoSSe sheet, vdW contribution was included with the Grimme's scheme (DFT-D3).[48] A vacuum spacing of 15 Å was placed between each adjacent images. Transition states along the reaction pathways were searched by Climbing Image Nudged Elastic Band (CI-NEB) approach.[49] The interaction between molecule and the substrate was described by the adsorption energy, which is expressed as,

$$E_{ad} = E_{sub+mol} - E_{sub} - E_{mol} \quad (1)$$

where $E_{sub+mol}$, E_{sub}, and E_{mol} are the total energy of the molecule adsorbed at substrate, isolated substrate, and isolated molecule in the same simulation box, respectively.

Results and discussions

The adsorption of water molecule at defective Janus MoSSe sheet

The primitive cell of Janus MoSSe sheet is a hexagonal structure as denoted by the green line see Fig. 1(a), which consists of S–Mo–Se atomic tri-layers with the upper Se, middle Mo, and lower S atoms as shown in Fig. 1(b). The relaxed cell of Janus MoSSe is in *P*3*m*1 space group, and the Mo atom is in six-fold, and the S (Se) atom is in three-fold coordinated. Here,

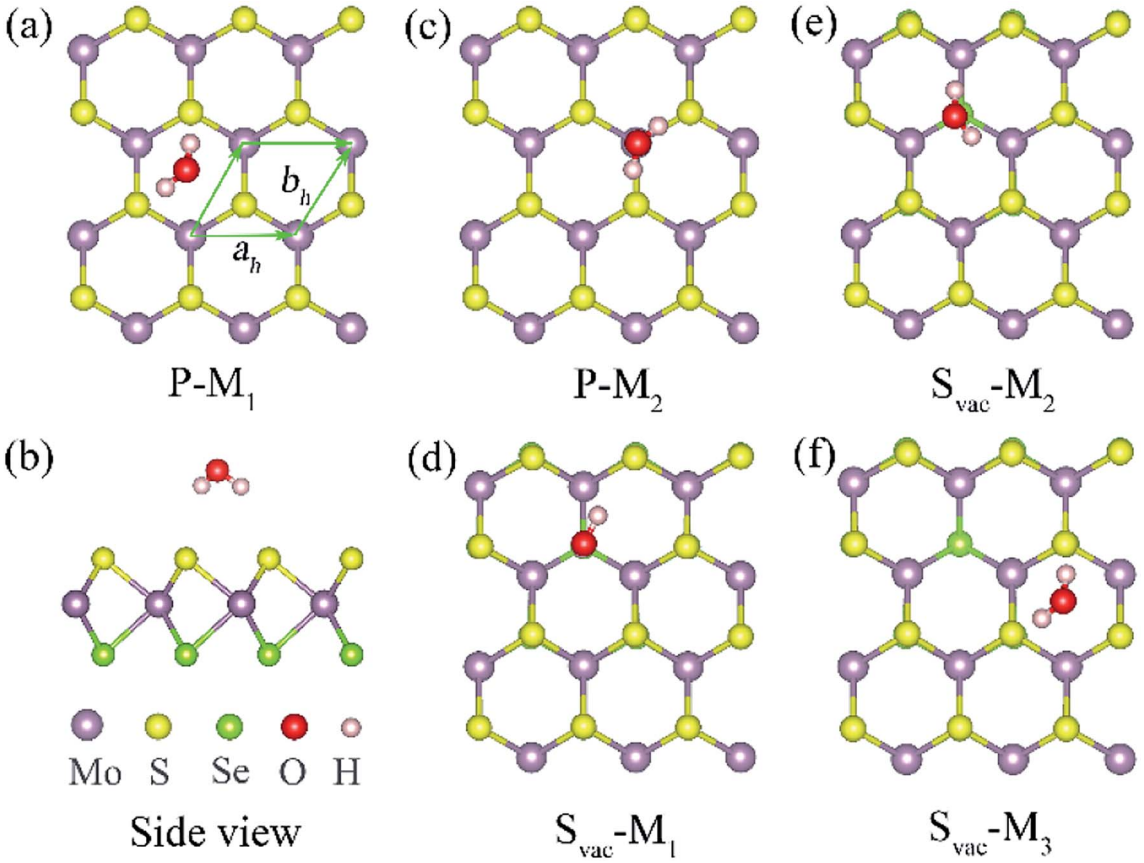

Fig. 1 Optimized structures for single water molecule adsorbed at a (4 × 4) Janus MoSSe sheet. (a) and (c) top views of possible water adsorption configurations, and (b) the corresponding side view of (a) at pristine case. (d)–(f) the top views of possible water adsorption structures at S_{vac} Janus MoSSe sheet. The primitive cell is denoted in green line. The Mo atom is light violet ball, S atom is yellow ball, Se is light green ball, O atom is red ball, and H atom is light pink ball for water adsorbed Janus MoSSe sheet, hereinafter.

a (4 × 4) supercell is used to model the Janus MoSSe sheet for water adsorption as shown in Fig. 1. For comparison, the molecular water (M-H_2O) adsorbed at pristine Janus MoSSe and MoS_2 sheet are firstly considered. The S side of the MoSSe is firstly examined, and there are two possible adsorption configurations existing after relaxation, denoted as P-M_1 and P-M_2 respectively, as shown in Fig. 1. In P-M_1, the H_2O is adsorbed at hollow site surrounded by three Mo atoms with H atoms pointing to S atoms (Fig. 1(a)). In P-M_2, the H_2O is adsorbed vertically over a single lattice Mo (Fig. 1(c)). The calculated adsorption energy for P-M_1 is −0.243 eV, which is 0.04 eV more negative than that of P-M_2, suggesting P-M_1 is slightly more stable. This result agrees well with the previous PBE prediction of 0.16 eV.[30] Similar to S side, the water adsorption on Se side of MoSSe is about −0.240 eV, which is a little smaller than that of S side. As for MoS_2 sheet, the adsorption of water is smaller than the above two with the value at about −0.219 eV. In all, we can find the adsorption energy of water on these three cases are quite close, where S side of MoSSe sheet has the largest water adsorption energy still a weak vdW interaction. The larger adsorption of water consistent with the shorter H–S bond length. Therefore, in the text, we choose S side of MoSSe as the typical one to investigate the water behavior.

It has been reported that defect introduction is an effectively approach to alter the surface reactivity. Here, intrinsic defects including S vacancy (S_{vac}), Mo antidefect (Mo_{anti}), and Mo interstitial (Mo_{int}) are considered for the Janus MoSSe sheet. It should be noted that only S side is considered, since the property of Se side is similar to that of S side. Firstly, one S_{vac} defect is introduced in the (4 × 4) supercell. Three typical water adsorption configurations are obtained from the geometry optimization calculations, denoted as S_{vac}-M_n (n = 1, 2, 3) as shown in Fig. 1. In S_{vac}-M_1, one H atom of M-H_2O is located at the S_{vac}, and the other H atom is pointing to the adjacent S atom in Fig. 1(d). In S_{vac}-M_2, the O atom of M-H_2O resides at the S_{vac} with the two H atoms pointing outwards. In S_{vac}-M_3, the M-H_2O is absorbed at a hexagonal hollow site that is away from S_{vac}. The corresponding calculated adsorption energies for S_{vac}-M_n are provided in Table 1. It is shown that the M-H_2O at S_{vac}-M_1 has the most negative adsorption energy of −0.321 eV, which is about 0.08 eV more negative than the M-H_2O adsorption energy for the pristine sheet. This more negative adsorption energy of S_{vac}-M_1, as compared to P-M_1, is consistent with substantially shorter Mo–H distance of 3.19 Å for S_{vac}-M_1 (*vs.* 4.29 Å for P-M_1). To know the difference between MoSSe and MoS_2 sheet, the water adsorbed at S_{vac} defect MoS_2 sheet is also examined. The result shows that the adsorption energy is about −0.297 eV at

Table 1 The adsorption energy (E_{ad}), and the corresponding relaxed geometry parameters of water adsorbed at pristine and S_{vac} Janus MoSSe sheet

System	M-H_2O	E_{ad}	H–S (Å)	H–Mo (Å)	O–H (Å)	∠HOH (degree)
Pristine	P-M_1	−0.243	2.661	4.290	0.972	103.414
	P-M_2	−0.239	2.645		0.972	103.35
	M-H_2O				0.97	104.131
S_{vac}	S_{vac}-M_1	−0.321	2.985	3.190	0.971	103.187
	S_{vac}-M_2	−0.307	2.879	3.397	0.972	103.262
	S_{vac}-M_3	−0.230	2.658	4.290	0.972	103.492

S_{vac} MoS_2, which is a little lower than that at S_{vac}_MoSSe sheet. Thus, introducing S_{vac} defect will slightly enhance the water adsorption on the Janus MoSSe sheet.

Other than S_{vac} defect, anti-defect is also considered by replacing one S atom by a Mo atom in the (4 × 4) supercell of the Janus MoSSe sheet. Three kinds of Mo_{anti} defects are allowed for by the (4 × 4) supercell, and the corresponding relaxed structures are denoted as Mo_{anti}-n (n = 1, 2, 3) as shown in Fig. 2. In Mo_{anti}-1, the Mo substitute resides at the exact position of the replaced S and forms three equal Mo–Mo bonds (Fig. 2(a)). In Mo_{anti}-2, the Mo substitute is slightly displaced towards the hollow center, forming two Mo–S and two Mo–Mo bonds (Fig. 2(b)). In Mo_{anti}-3 the Mo substitute is slightly displaced towards the adjacent lattice Mo, forming two Mo–S bonds and a Mo–Mo bond in Fig. 2(c). Among these three configurations, Mo_{anti}-2 defect is found to be more stable, as suggested by the predicted relative energies (Table 2).

The adsorption of molecular water at the $Mo_{anti\text{-}2}$ site is investigated. Three adsorption configurations are resulting from the geometry optimization calculations, denoted as Mo_{anti}-2-M_n (n = 1, 2, 3), as shown in Fig. 2. In Mo_{anti}-2-M_1, the M-H_2O is tiltedly adsorbed at Mo_{anti} atom site with H atoms pointing to the two nearest S atom. In Mo_{anti}-2-M_2, the M-H_2O resides right atop the Mo_{anti} atom with H atoms pointing to two nearest S atoms. Mo_{anti}-2-M_3 is structurally close to Mo_{anti}-2-M_1 except for the pointing directions of the H atoms. The

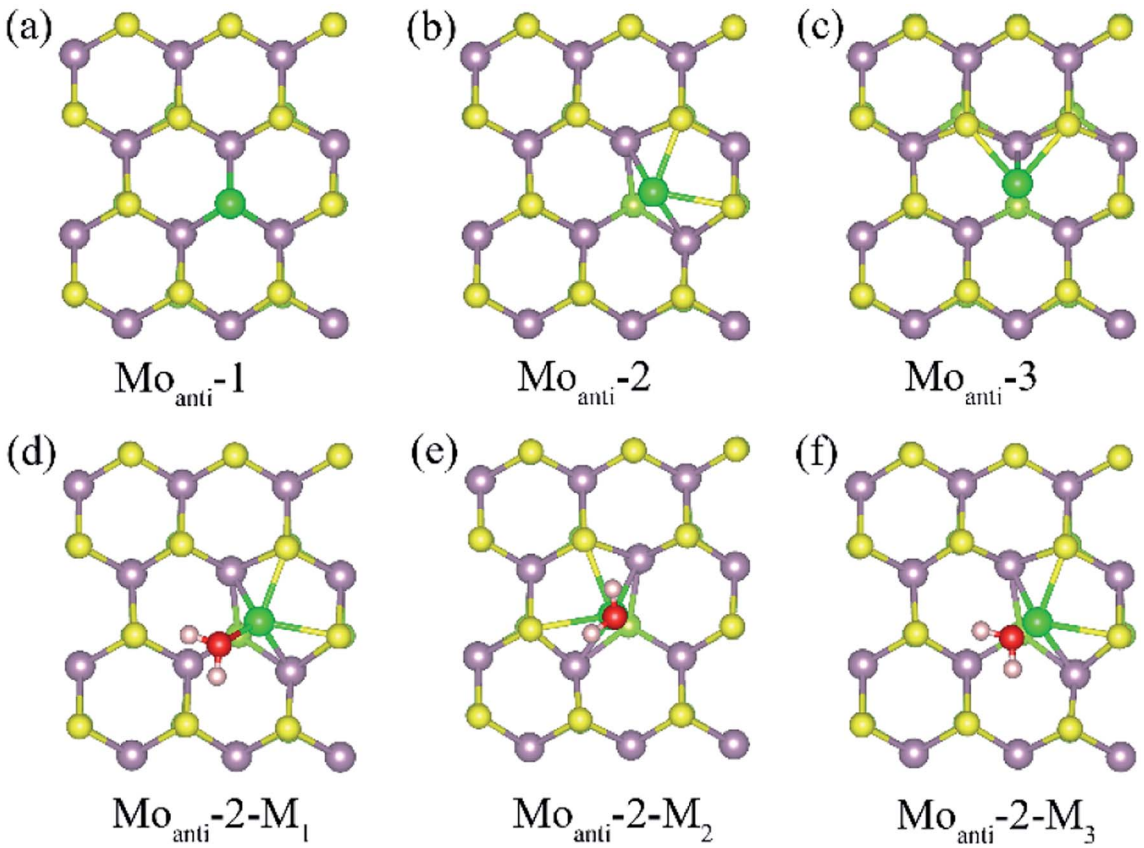

Fig. 2 (a)–(c) The possible Mo_{anti} defect at Janus MoSSe sheet. (d)–(f) The water molecule adsorption at Mo_{anti}-2 structure. The Mo_{anti} atom is in green ball.

Table 2 The relative energy of Mo_{anti} or Mo_{int} defect at possible site in Janus MoSSe sheet. The corresponding relaxed geometry parameters are also provided. It should be mentioned that the relative lower total energy is set to zero point

Defect type	Localized sites	Relative energy	Mo–Mo (Å)	Mo–S (Å)
Mo_{anti}	Mo_{anti}-1	0.450	2.522	3.115
	Mo_{anti}-2	0	2.430	2.443
	Mo_{anti}-3	0.366	2.439	2.457
Mo_{int}	Mo_{int}-1	0.127	2.881	2.194
	Mo_{int}-2	0	2.443	2.430

Table 3 The calculated adsorption energy (E_{ad}), and the corresponding relaxed geometry parameters of water molecule adsorbed at Mo_{anti} or Mo_{int} defective Janus MoSSe sheet

System	M-H_2O	E_{ad}	H–S (Å)	O–Mo (Å)	O–H (Å)	∠HOH (°)
Mo_{anti}-2	Mo_{anti}-M_1	−1.415	2.324	2.199	0.937	102.650
	Mo_{anti}-M_2	−1.061	2.905	2.228	0.978	106.704
	Mo_{anti}-M_3	−1.203	2.610	2.228	0.981	104.163
Mo_{int}-2	Mo_{int}-M	−1.202	2.418	2.295	0.975	103.501

corresponding adsorption energy and relaxed geometry parameters for the three configurations are shown in Table 3. It can be found that the adsorption energies of M-H_2O at all three modes are more negative than −1.0 eV. Among the three configurations, Mo_{anti}-2-M_1 has the most negative M-H_2O adsorption energy (−1.42 eV), together with the shortest Mo–O distance of ∼2.2 Å. Relative to M-H_2O at pristine sheet, it is unexpected to find that the adsorption energy is dramatically increased by −1.18 eV. Furthermore, the difference between MoSSe and MoS_2 sheet are checked. Compared with Mo_{anti} MoSSe, the water adsorption at Mo_{anti} MoS_2 is about 0.036 eV larger than that at MoSSe sheet, suggesting Mo_{anti} defect at MoSSe has larger effect on water adsorption. Therefore, Mo_{anti} defect can strongly alter the adsorption behavior of water at Janus MoSSe sheet, which would be a potential way to promote the photocatalytic water splitting.

Interstitial defect is another common intrinsic defect type for transition metal dichalcogenides. The models for Janus MoSSe with Mo_{int} defect are constructed by adding one Mo atom to the (4 × 4) supercell. Two types of Mo_{int} defects are obtained from the geometry optimization calculations, denoted as Mo_{int}-1 and Mo_{int}-2, as shown in Fig. 3. For Mo_{int}-1, the Mo_{int} atom is located at hollow site forming three Mo–S bonds. In Mo_{int}-2, the Mo_{int} atom is located right atop the lattice Mo atom forming three Mo–S bonds. Although the Mo_{int} atom at Mo_{int}-2 seems repulsively with lattice Mo atom, the calculated relative energy shows Mo_{int}-2 is about 0.13 eV lower than that of Mo_{int}-1, suggesting Mo_{int}-2 is more stable.

Based on the comparatively more stable Mo_{int}-2 structure, the behavior of M-H_2O adsorption at Mo_{int} defective MoSSe sheet is investigated, and the corresponding calculated result is displayed in Table 3. Only one type of M-H_2O adsorption configuration is found, denoted as Mo_{int}-M (Fig. 3). The corresponding M-H_2O adsorption energy for Mo_{int} defective sheet is about −1.2 eV, comparable to that for the Mo_{anti} defective sheet. Furthermore, the difference between MoSSe and MoS_2 sheet are checked. Compared with Mo_{int} MoSSe, the water adsorption at Mo_{int} MoS_2 is close to that at MoSSe sheet, suggesting Mo_{anti} defect at both MoSSe and MoS_2 sheet has identical effect on water adsorption. Thus, Mo_{int} defect can also effectively enhance water adsorption at defective MoSSe sheet. In all, the S_{vac} defect can slightly increase the water adsorption, while Mo_{anti} and Mo_{int} can significantly enhance the interaction between water molecule and substrate.

The adsorption behavior of dissociated water at defective Janus MoSSe sheet

Above result shows the intrinsic defects have a prominent effect on the adsorption of water molecule at Janus MoSSe sheet. In order to know whether these defects could affect the water splitting, the adsorption behavior of dissociated water (D-H_2O) is also explored. According to the possible atomic site, two types of D-H_2O modes are existing for each defective MoSSe sheet as shown in Fig. 4. As for S_{vac} defective sheet, the relaxed configuration of D-H_2O can be denoted as S_{vac}-D_n (n = 1, 2) for short. For example, the H atom of D-H_2O in S_{vac}-D_1 is forming H–S

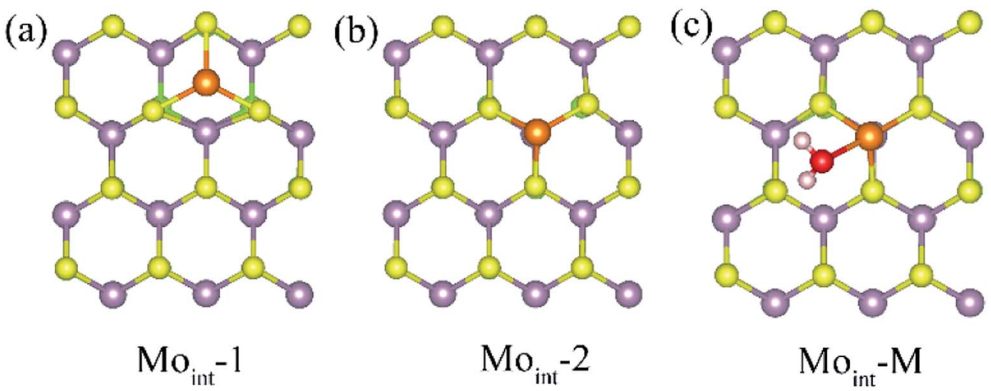

Fig. 3 (a) and (b) The top view of possible Mo_{int} defect at Janus MoSSe sheet. (c) The adsorption of molecular water at Mo_{int} MoSSe sheet. The Mo_{int} atom is light orange ball.

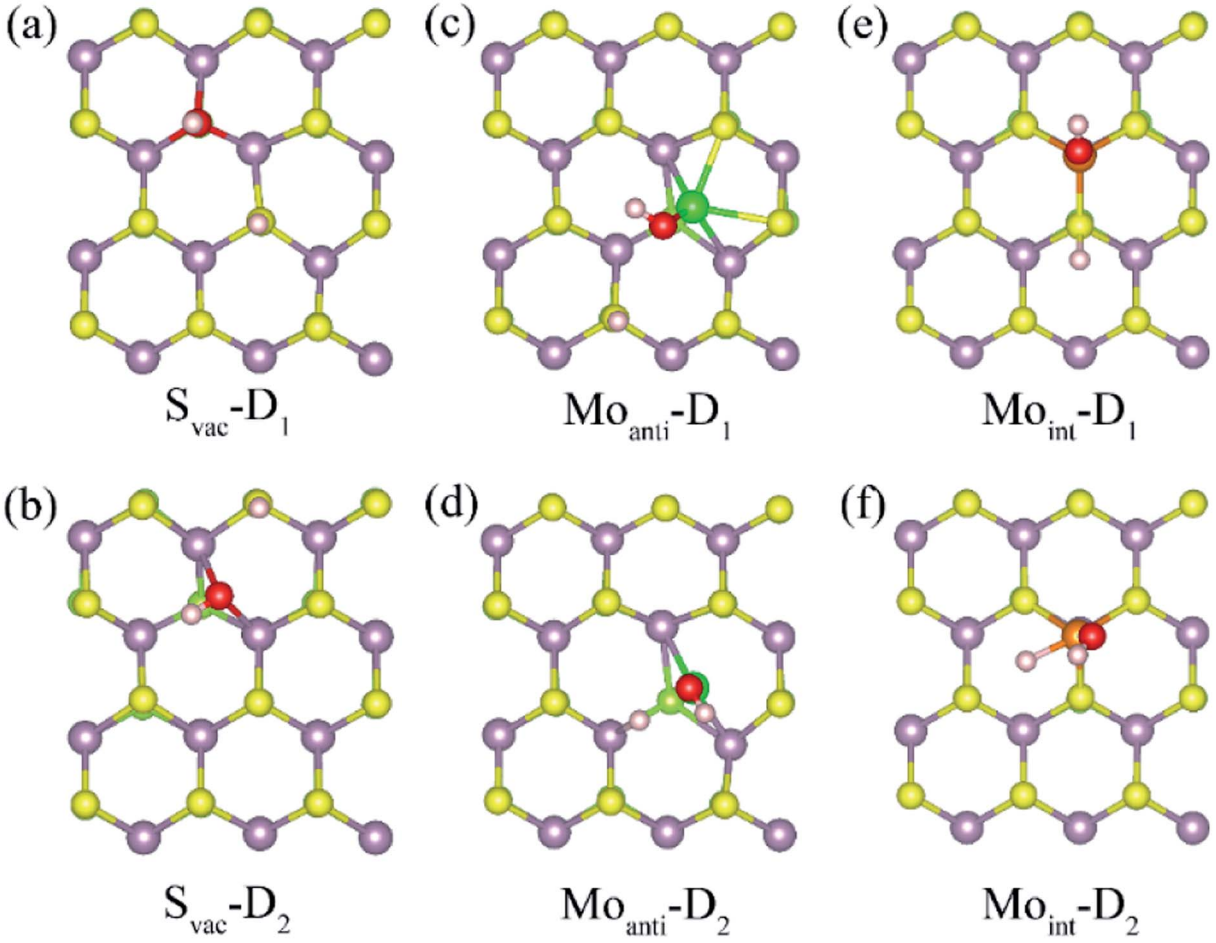

Fig. 4 The relaxed structures of dissociated water at defective Janus MoSSe sheet. The top view of dissociated water at S_{vac} (a) and (b), Mo_{anti} (c), (b), and Mo_{int} (e), (f) defective Janus MoSSe sheet.

next to S_{vac} defect, while the OH is located at the site of S_{vac} forming three Mo–O bonds. In S_{vac}-D_1, it forms two Mo–O bonds for S_{vac}-D_2. The case for Mo_{anti} defect is quite different because of the unsaturated bonds of lattice Mo atom near Mo_{anti} defect. Thus, it can form two different configurations of D-H_2O with the H linked to lattice S atom in Mo_{anti}-D_1 or to lattice Mo atom in Mo_{anti}-D_2. As for D-H_2O at Mo_{int} defect sheet, the H of D-H_2O is linked to S atom next to Mo_{int} atom in Mo_{int}-D_1, while both the OH and H atoms are directly absorbed to Mo_{int} atom in Mo_{int}-D_2.

The calculated adsorption energy, energy difference, and the corresponding relaxed geometry parameters are displayed in Table 4. Surprisingly, it can be found that the adsorption energy of D-H_2O at S_{vac} Janus MoSSe sheet is positive, where S_{vac}-D_3 has a relative lower adsorption energy at about 0.658 eV. In order to check whether the M-H_2O favors to form D-H_2O, the energy difference between M-H_2O and D-H_2O is provided. The result shows that the energy difference is 0.985 eV for water at S_{vac} defect sheet, showing M-H_2O is more stable. Thus, the water molecule may be difficult to split at S_{vac} Janus MoSSe sheet. As for water on Mo_{anti} defect sheet, the adsorption energies for D-H_2O are negative, with Mo_{anti}-D_2 lower adsorption energy at about −1.625 eV. Moreover, it is interesting to find that the energy difference is a negative value of −0.21 eV, indicating D-H_2O is more stable. Thus, the molecular water may be favored to dissociate at Mo_{anti} defect sheet. Similar to the case at Mo_{anti} defect sheet, the adsorption energy for D-H_2O at Mo_{int} defective Janus MoSSe sheet are all negative. And the energy difference is about −0.993 eV, which is larger than the case at Mo_{anti} sheet at about −0.21 eV. The lower adsorption energy of D-H_2O is related

Table 4 The calculated adsorption energy (E_{ad}), and the corresponding relaxed geometry parameters of D-H_2O at defective Janus MoSSe sheet. The energy difference (E_{dif}) is the total energy difference between M-H_2O and D-H_2O, and the negative value means D-H_2O is more stable

System	D-H_2O	E_{ad}	E_{dif}	H–S	O–Mo	O–H
S_{vac}	S_{vac}-D_1	0.664	0.985	1.359	2.177	0.983
	S_{vac}-D_2	0.896	1.217	1.36	2.201	1.003
Mo_{anti}-2	Mo_{anti}-D_1	−0.800	0.615	1.362	1.914	0.978
	Mo_{anti}-D_2	−1.625	−0.209	1.778 (H–Mo)	1.916	0.977
Mo_{int}-2	Mo_{int}-D_1	−1.414	−0.211	1.389	1.901	0.971
	Mo_{int}-D_2	−2.195	−0.993	1.679 (H–Mo)	1.892	0.972

with shorter Mo–O bond length. For example, the bond length of Mo–O at S_{vac}-D_1 sheet is changing from 2.117 Å to 1.91 Å for Mo_{anti}-D_2, even shorten to 1.892 Å for Mo_{int}-D_2. Therefore, the Mo_{anti} and Mo_{int} defects can greatly enhance the adsorption energy of D-H_2O, which may promote the process of photocatalytic water splitting.

Discussion

The above result shows that the intrinsic defects can dramatically enhance the interaction between water and Janus MoSSe sheet. To check the role of these defects, the structural and electronic property of intrinsic defects are discussed. First of all, the structural parameter of the defective structure is examined, since introducing defect will induce local structure distortion. It can be found that the bond length of Mo–S around the defect will be strongly shrunk, where it is shorten by 0.02 Å for S_{vac} and 0.17 Å for Mo_{int} defect sheet. Furthermore, these defects will introduce unsaturated Mo atom at the Janus MoSSe sheet, which will enhance the reactivity of sheet.

Except for the local structure distortion, the electronic structures of the defective structure are also examined since defects provide unique electronic property, which are crucial to the reactivity of surface. Here, the projected partial electronic density of state (PDOS) for defective Janus MoSSe sheet adsorbed with molecular water are calculated together with pristine case for comparison, and the corresponding calculated result is shown in Fig. 5. It should be noted that only the electronic density of states for Mo, S, O, and H atoms are provided, since the water is adsorbed at S side. For pristine sheet, we can find that the PDOS of adsorbed water remains in three intact peaks similar to single water molecule. This strongly suggests that the adsorbed water is hardly interact with pristine Janus MoSSe sheet, corresponding to weak adsorption energy of −0.16 eV.[30] As a S_{vac} defect exists in the structure, the three peaks are almost preserved, but the location of the peaks have a little red shift toward lower energy level, suggesting water adsorption is more favored corresponding larger adsorption energy of −0.23 eV. The case for Mo_{anti} and Mo_{int} defects are much different. First of all, it is unexpected to find that the three peaks disappear, and the PDOS of adsorbed water disperses into a large area, suggesting a strong interaction between O2p orbital of water with Mo3d orbitals of Mo_{anti} or Mo_{int} defect. Furthermore, the PODS of the adsorbed water is dispersed in the arrange from −6.6 eV to −5.0 eV for Mo_{anti} defect, and −6.0 eV to −5.2 eV for Mo_{int} defect sheet. Thus, a dramatic red shift of the PDOS for the adsorbed water is relative to the water adsorbed at pristine Janus MoSSe sheet. This results in larger adsorption energy of water at Mo_{anti} or Mo_{int} defect Janus MoSSe sheet with the value of −1.4 eV or 1.2 eV. Therefore, the origin of enhanced adsorption energy of water at defective S side of sheet should be the orbitals interaction between O2p of water and Mo3d of defects, together with the red shift of water energy level.

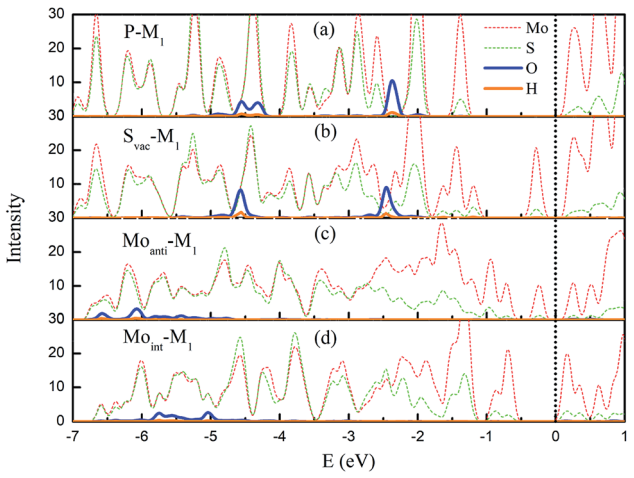

Fig. 5 The projected partial electronic density of states (PDOS) of the M-H_2O adsorbed at defective MoSSe sheet. The PDOS of H_2O adsorbed at pristine Janus MoSSe sheet is also provided in (a) for comparison. (b)–(d) represent the PDOS of M-H_2 adsorbed at S_{vac}, Mo_{anti}, and Mo_{int} defective MoSSe sheet, respectively. The PDOS of Mo, S, O, and H atoms are in red (short dash), green (short dash), blue, and orange lines. The black dot line denotes the VBM, which is setting at zero eV.

Conversion of water at defective Janus MoSSe sheet

As mentioned in introduction, Janus MoSSe sheet is a promising photocatalyst for water splitting, however it is limited by the weak water adsorption. Fortunately, the above result shows that S_{vac}, Mo_{anti} and Mo_{int} intrinsic defects can greatly enhance the adsorption of water at Janus MoSSe sheet. Thus, it is of interest to know the effect of intrinsic defect on water conversion. Generally, it involves both the most stable M-H_2O state and D-H_2O state during the water splitting process, which can be expressed as:

$$H_2O \rightarrow H^+ + OH^- \quad (2)$$

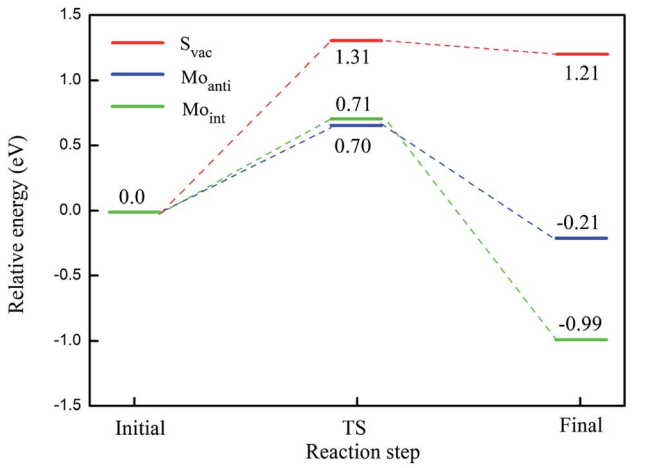

Fig. 6 Illustration of reaction pathway *via* M-H_2O to form H and OH bond. The sum of energies of the water and substrate is the zero reference for energy. The transition state is denoted as TS for short. The relative energy for water splitting at S_{vac}, Mo_{anti}, and Mo_{int} defect sheet are in red, blue, and green lines, respectively.

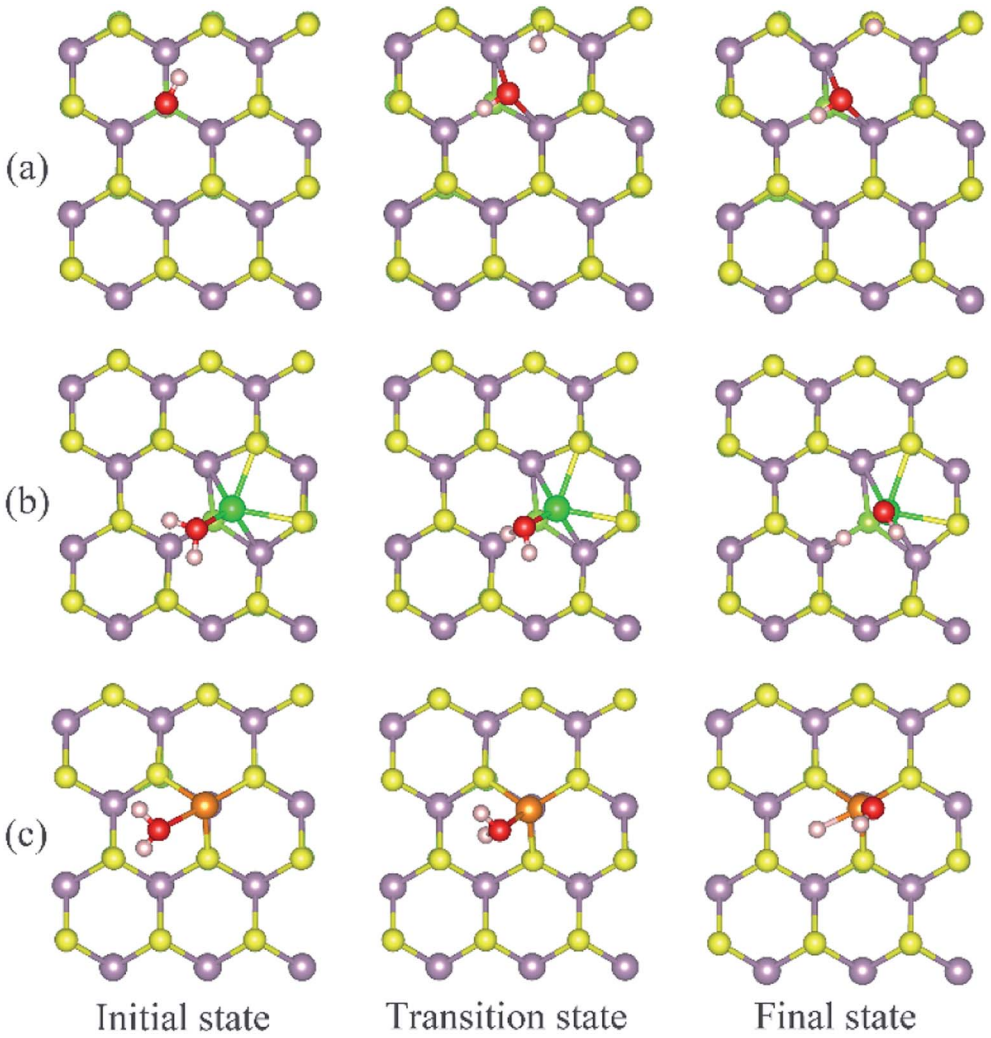

Fig. 7 Selected configurations along the conversion pathway of water at defective Janus MoSSe sheet. The detailed defects are displayed in (a) S_{vac}, (b) Mo_{anti}, and (c) Mo_{int} defective Janus MoSSe sheet.

This reaction process involves two steps with the water molecule adsorbed at the Janus MoSSe sheet; consecutively, one H of M-H_2O transfers to lattice S or Mo atom to form H–S or Mo–H bond, leaving OH bond at the sheet.

The calculated energy barrier of water conversion to H and OH at defective Janus MoSSe sheet are shown in Fig. 6. It should be mentioned that D-H_2O is unable to form at pristine Janus MoSSe sheet. Thus, we only consider the water conversion at the defective sheet. The result shows that it requires 1.31 eV energy to overcome the transition state for water splitting at S_{vac} defect sheet. During this process, the H atom of water towards to the adjacent lattice S atom through a transition state to form an H–S bond and an O–H bond as shown in Fig. 7(a). Additionally, the final state of D-H_2O is a little lower than that of transition state, but 1.21 eV larger than initial state of M-H_2O. Thus, water may be difficult to split at S_{vac} defect Janus MoSSe sheet.

Compared to S_{vac} defect, the behavior of other defects such as Mo_{anti} and Mo_{int} defects appears completely different. For example, for Mo_{anti} defect, one H atom of water links to unsaturated lattice Mo atom through a transition state as shown in Fig. 7(b). The corresponding energy barrier for the water splitting is about 0.71 eV, which is dramatically lower than that at S_{vac} sheet. Furthermore, it is interesting to find that the relative energy of the final state is about 0.21 eV lower than the initial state. As for Mo_{int} defect, it has larger impact than S_{vac} and Mo_{anti} defects on water splitting. The H atom of water towards to Mo_{int} atom forming Mo–H bond as shown in Fig. 7(c). The calculated result shows that it needs 0.7 eV to overcome the transition state, close to the case at Mo_{anti} sheet. Interestingly, the final state of D-H_2O is about −0.99 eV, extremely lower than the initial state. Therefore, the Mo_{anti} and Mo_{int} defects have greatly impact on decreasing the energy barrier of water splitting, indicating introducing defect should be a promising approach to modify the reactivity of low dimensional materials.

Conclusion

In summary, the first-principles calculations are carried out to explore the effect of intrinsic defects on water adsorption and conversion at Janus MoSSe sheet. The result shows that relative

to pristine case, the adsorption energy of M-H_2O increases to −0.32 eV under S_{vac} defect, while D-H_2O is difficult to form. Unlike S_{vac} defect, the effect of Mo_{anti} and Mo_{int} defect is much stronger than S_{vac} defect on water behavior at Janus MoSSe sheet. The water adsorption energy at both Mo_{anti} and Mo_{int} sheet can be increased by −1.0 eV. More importantly, the energy barrier for water splitting can be lowered by 40% to 0.7 eV at Mo_{anti} or Mo_{int} defects sheet, and the final state of D-H_2O is stable than the initial state. This significant enhancement of the adsorption energy originates from the strong interaction between O2p orbital and Mo3d orbitals. These results presented here showed that the intrinsic defect has the potential to change the property of materials, thus it is an important way to design photocatalyst for water splitting.

Conflicts of interest

There are no conflicts to declare.

Acknowledgements

This work was supported by the Science Challenge Project (TZ2018004) and the National Natural Science Foundation of China (No. 51572016, U1930402, 11804090, 11847213, 11774298, and 21503012). It is supported by the Scientific Research Fund of Hunan provincial Education Department, China (Grant No. 17C0626, and 2019JJ50148), and Scientific Research Fund of University (No. E517558). This research is supported by a Tianhe-2JK computing time award at the Beijing Computational Science Research Center (CSRC) and the Special Program for Applied Research on Super Computation of the NSFC Guangdong Joint Fund (the second phase) under Grant No. U1501501.

References

1 Yin, B. Wen, C. Zhou, A. Selloni and L.-M. Liu, *Surf. Sci. Rep.*, 2018, **73**, 58.
2 K. Wenderich and G. Mul, *Chem. Rev.*, 2016, **116**, 14587.
3 J. Su, Y. Wei and L. Vayssieres, *J. Phys. Chem. Lett.*, 2017, **8**, 5228.
4 M. Kapilashrami, Y. Zhang, Y. S. Liu, A. Hagfeldt and J. Guo, *Chem. Rev.*, 2014, **114**, 9662.
5 J. Schneider, M. Matsuoka, M. Takeuchi, J. Zhang, Y. Horiuchi, M. Anpo and D. W. Bahnemann, *Chem. Rev.*, 2014, **114**, 9919.
6 Y. Yang, *et al.*, *Adv. Mater.*, 2018, **30**, 1704479.
7 R. Li, Y. Weng, X. Zhou, X. Wang, Y. Mi, R. Chong, H. Han and C. Li, *Energy Environ. Sci.*, 2015, **8**, 2377.
8 W. J. Ong, L. L. Tan, Y. H. Ng, S. T. Yong and S. P. Chai, *Chem. Rev.*, 2016, **116**, 7159.
9 P. Miro, M. Ghorbani-Asl and T. Heine, *Angew. Chem., Int. Ed. Engl.*, 2014, **53**, 3015.
10 Z. Tan, *et al.*, *J. Am. Chem. Soc.*, 2016, **138**, 16612.
11 R. Li, L. Zhang, L. Shi and P. Wang, *ACS Nano*, 2017, **11**, 3752.
12 F. Shayeganfar, K. S. Vasu, R. R. Nair, F. M. Peeters and M. Neek-Amal, *Phys. Rev. B*, 2017, **95**, 144109.
13 W. J. Ong, L. L. Tan, Y. H. Ng, S. T. Yong and S. P. Chai, *Chem. Rev.*, 2016, **116**, 7159.
14 R. K. Joshi, S. Shukla, S. Saxena, G. H. Lee, V. Sahajwalla and S. Alwarappan, *AIP Adv.*, 2016, **6**, 015315.
15 W. Li, Z. Lin and G. Yang, *Nanoscale*, 2017, **9**, 18290.
16 Y.-N. Z. Hui Zhang, H. Liu and Li-M. Liu, *J. Mater. Chem. A*, 2014, **2**, 15389.
17 Q. Xiang, J. Yu and M. Jaroniec, *J. Am. Chem. Soc.*, 2012, **134**, 6575.
18 W. S. Yun, S. W. Han, S. C. Hong, I. G. Kim and J. D. Lee, *Phys. Rev. B*, 2012, **85**, 033305.
19 S. Fathipour, *et al.*, *Appl. Phys. Lett.*, 2014, **105**, 192101.
20 B. Radisavljevic, A. Radenovic, J. Brivio, V. Giacometti and A. Kis, *Nat. Nanotechnol.*, 2011, **6**, 147.
21 K.-A. N. Duerloo, M. T. Ong and E. J. Reed, *J. Phys. Chem. Lett.*, 2012, **3**, 2871.
22 L. Dong, J. Lou and V. B. Shenoy, *ACS Nano*, 2017, **11**, 8242.
23 Y. Guo, S. Zhou, Y. Bai and J. Zhao, *Appl. Phys. Lett.*, 2017, **110**, 163102.
24 X. Li, Z. Li and J. Yang, *Phys. Rev. Lett.*, 2014, **112**, 018301.
25 H. Yang, P. Zhao, Y. Ma, X. Lv, B. Huang and Y. Dai, *J. Appl. Phys.*, 2019, **52**, 455303.
26 X. Gao, Y. Shen, Y. Ma, S. Wu and Z. Zhou, *Inorg. Chem.*, 2019, **58**, 12053.
27 A.-Y. Lu, *et al.*, *Nat. Nanotechnol.*, 2017, **12**, 744.
28 C. Shang, B. Xu, X. Lei, S. Yu, D. Chen, M. Wu, B. Sun, G. Liu and C. Ouyang, *Phys. Chem. Chem. Phys.*, 2018, **20**, 20919.
29 W.-J. Yin, B. Wen, Q.-X. Ge, G.-Z. Nie, X.-L. Wei and L.-M. Liu, *J. Mater. Chem. C*, 2018, **6**, 1693.
30 X. Ma, X. Wu, H. Wang and Y. Wang, *J. Mater. Chem. A*, 2018, **6**, 2295.
31 H. U. Din, M. Idrees, A. Albar, M. Shafiq, I. Ahmad, C. V. Nguyen and B. Amin, *Phys. Rev. B*, 2019, **100**, 165425.
32 W. Yin, B. Wen, Q. Ge, D. Zou, Y. Xu, M. Liu, X. Wei, M. Chen and X. Fan, *Prog. Nat. Sci.: Mater. Int.*, 2019, **29**, 335.
33 Z. Guan, S. Ni and S. Hu, *J. Phys. Chem. C*, 2018, **122**, 6209.
34 W.-J. Yin, M. Krack, B. Wen, S.-Y. Ma and L.-M. Liu, *J. Phys. Chem. Lett.*, 2015, **6**, 2538.
35 W.-J. Yin, B. Wen, Q.-X. Ge, X.-L. Wei, M. Chen and L.-M. Liu, *Comput. Mater. Sci.*, 2018, **155**, 424.
36 J. Sá, C. Garlisi, G. Palmisano, J. Czapla-Masztafiak, Y. Kayser and J. Szlachetko, *Mater. Chem. Phys.*, 2018, **208**, 281.
37 F. Gunkel, *et al.*, *Phys. Rev. X*, 2016, **6**, 031035.
38 Y. Wang, J. Zhao, T. Wang, Y. Li, X. Li, J. Yin and C. Wang, *J. Catal.*, 2016, **337**, 293.
39 X. Ma, X. Yong, C.-c. Jian and J. Zhang, *J. Phys. Chem. C*, 2019, **123**, 18347.
40 D. Merki, H. Vrubel, L. Rovelli, S. Fierro and X. Hu, *Chem. Sci.*, 2012, **3**, 2515.
41 X. Zhang, *et al.*, *Mater. Res. Express*, 2019, **6**, 105055.
42 K. Zhang, *et al.*, *Nano Lett.*, 2017, **17**, 6676.
43 Z. Wang, L. Chu, L. Li, M. Yang, J. Wang, G. Eda and K. P. Loh, *Nano Lett.*, 2019, **19**, 2840.
44 R. Chaurasiya and A. Dixit, *Appl. Surf. Sci.*, 2019, **490**, 204.

45 J. VandeVondele, M. Krack, F. Mohamed, M. Parrinello, T. Chassaing and J. Hutter, *Comput. Phys. Commun.*, 2005, **167**, 103.
46 M. Krack, *Theor. Chem. Acc.*, 2005, **114**, 145.
47 J. Heyd, G. E. Scuseria and M. Ernzerhof, *J. Chem. Phys.*, 2006, **124**, 219906.
48 J. A. Stefan Grimme, S. Ehrlich and H. Krieg, *J. Chem. Phys.*, 2010, **132**(1), 154104.
49 G. Henkelman and H. Jónsson, *J. Chem. Phys.*, 2000, **113**, 9978.